

*Annual Review of Materials Research*  
Electronic, Ionic, and  
Mixed Conduction in  
Polymeric Systems

Elayne M. Thomas,<sup>1</sup> Phong H. Nguyen,<sup>2</sup>  
Seamus D. Jones,<sup>2</sup> Michael L. Chabinyc,<sup>1</sup>  
and Rachel A. Segalman<sup>1,2</sup>

<sup>1</sup>Materials Department, University of California, Santa Barbara, California 93106, USA; email: ethomas@ucsb.edu, mchabinyc@engineering.ucsb.edu, segalman@engineering.ucsb.edu

<sup>2</sup>Department of Chemical Engineering, University of California, Santa Barbara, California 93106, USA; email: php@ucsb.edu, seamusdjohnes@ucsb.edu

Annu. Rev. Mater. Res. 2021. 51:1–20

First published as a Review in Advance on  
March 26, 2021

The *Annual Review of Materials Research* is online at  
matsci.annualreviews.org

<https://doi.org/10.1146/annurev-matsci-080619-110405>

Copyright © 2021 by Annual Reviews.  
All rights reserved

ANNUAL  
REVIEWS **CONNECT**

[www.annualreviews.org](http://www.annualreviews.org)

- Download figures
- Navigate cited references
- Keyword search
- Explore related articles
- Share via email or social media

### Keywords

polymers, mixed conduction, electrochemistry, transport models, structure-property relationships

### Abstract

Polymers that simultaneously transport electrons and ions are paramount to drive the technological advances necessary for next-generation electrochemical devices, including energy storage devices and bioelectronics. However, efforts to describe the motion of ions or electrons separately within polymeric systems become inaccurate when both species are present. Herein, we highlight the basic transport equations necessary to rationalize mixed transport and the multiscale material properties that influence their transport coefficients. Potential figures of merit that enable a suitable performance benchmark in mixed conducting systems independent of end application are discussed. Practical design and implementation of mixed conducting polymers require an understanding of the evolving nature of structure and transport with ionic and electronic carrier density to capture the dynamic disorder inherent in polymeric materials.

## 1. INTRODUCTION

The simultaneous transport of both electrons and ions is fundamental to the electrochemical processes that drive energy generation and storage devices. Several reviews have highlighted other applications for which mixed conduction is critical, including polymer-based bioelectronic and optoelectronic devices (1–3). Despite the potential importance of polymeric mixed conductors in these applications, a holistic understanding of mixed ionic and electronic conduction remains limited. Part of the knowledge gap arises from the unshared language between research communities. The design rules for ionic conduction are different than those for electronic conduction, which leads to difficulty when the conduction of both carriers is necessary.

Polymers, historically considered insulating, exhibit uniquely different transport behavior from their conducting ceramic and metallic counterparts. The mechanical properties and processability of polymers make them especially promising for improving device design. Both processing history and mechanical properties of polymers are intimately coupled to the conduction of ions and electrons; therefore, attaining both suitable conductivity and structural performance is challenging. Current design rules for polymers with high ionic or electronic mobility stem from studying these charged species separately. Ionic conductivity is coupled to polymer segmental motion and is therefore dominated by motion through the amorphous regions of a semicrystalline polymer (4). Conversely, electronic mobility is highest in more ordered domains of the polymer that allow for stronger electronic coupling between chains than in disordered domains (5). A critical challenge is to understand if conduction of two charge carrier types simply requires optimization of these orthogonal design requirements or if there are exploitable synergies between these conduction mechanisms.

Multicomponent mixed conducting polymer systems are often tailored to perform in hydrated, dry, or other environments. Differences in the intended application make it difficult to develop robust design principles for mixed conducting polymers that transcend their end use. The presence of added salts, solvents, and other additives to the polymer in a given mixed conducting system impacts the transport mechanisms for both the electrons and ions. For example, aqueous systems, such as hydrogels, polyelectrolytes, and poly[3,4-(ethylenedioxy)thiophene]:poly(styrenesulfonate) (PEDOT:PSS), typically exhibit ionic conductivity greater than  $10^{-3}$  S/cm, but the conductivity drops precipitously as the water content decreases below 50% by weight (6). Designs based on block copolymers and oligomers (7, 8), polymer blends (9, 10), and homopolymers (11, 12) with mixed ionic and electronic functionality have all been proposed. We choose not to focus on a specific mixed conductor architecture but identify a few examples of materials for which fundamental relationships have been found and discuss how their behavior can be generalized to other classes of polymers.

Herein, we review the efforts made to design and understand mixed conducting polymers. We highlight concepts and insights from the literature on ion- and electron-conducting polymers that are relevant to mixed conduction in a single materials system and show that simultaneous optimization of ion and electronic conduction requires new design rules. Section 2 describes the physics of ion- and electron-conducting polymeric systems. Section 3 describes the nomenclature and methods used to study these phenomena and efforts to describe simultaneous conduction in polymeric systems. Section 4 discusses directions and considerations for future research on these materials systems.

## 2. THE PRINCIPLES OF MIXED CONDUCTION

### 2.1. Transport Fundamentals

The mechanisms of ionic and electronic transport depend on electrostatic interactions of all charged species with the local electric field. Electronic charge conduction has been shown to range

from hopping-like to delocalized transport depending on the temperature and carrier concentration (13–15). Reported charge carrier mobilities are longer-range averages of fundamental local processes. In the same vein, localized liquid-like mechanisms are responsible for ion transport in ion-conducting polymers (16, 17). Thus, the transport of both ionic and electronic charge carriers can be described by a species balance around a control volume within a polymer system (18):

$$\partial c_i / \partial t = -\nabla \cdot \mathbf{N}_i + R_i, \quad 1.$$

where  $\partial c_i / \partial t$  is the rate of change of concentration,  $\nabla \cdot \mathbf{N}_i$  is the divergence of the flux through a control volume, and  $R_i$  is a term that accounts for the generation and consumption of species  $i$  (e.g., chemical reactions).

Mixed conducting polymers typically operate below the melting temperature, where both amorphous and crystalline phases exist. As such, the bulk of the system does not flow and the contributions of the velocity field to the flux can be neglected, as generation and consumption terms usually are. Frequently, the Nernst-Planck extension of Fick's law is used to describe the flux of ions and electronic charge carriers (18–22):

$$\mathbf{N}_i = -z_i \mu_i F c_i \nabla \Phi + c_i \mathbf{v} - D_i \nabla c_i, \quad 2.$$

where  $z_i$  is the integer charge,  $\mu_i$  is the mobility,  $F$  is the Faraday constant,  $c_i$  is the concentration,  $\nabla \Phi$  is the gradient of the electric potential,  $\mathbf{v}$  is the velocity field that the species moves with, and  $D_i$  is the diffusion coefficient.

From Equation 2, the net flux of either ions or electronic charge carriers is a linear sum of (a) drift (i.e., migration) due to the electric potential, (b) convection due to the velocity field, and (c) diffusion due to the concentration gradient.

An equivalent representation of current density for electronic charge carriers is given by Ohm's law (where  $\mathbf{v} = 0$  and  $\nabla c_i = 0$ ) (18),

$$\mathbf{j} = -\kappa \nabla \Phi, \quad \kappa = F^2 \sum z_i^2 \mu_i p_i, \quad 3.$$

where  $\mathbf{j}$  is the current density,  $\kappa$  is the conductivity,  $\nabla \Phi$  is the electric potential gradient,  $z_i$  is the integer charge,  $\mu_i$  is the mobility, and  $p_i$  is the charge carrier density (concentration).

To a first approximation, the diffusion and mobility of both ionic and electronic charge carriers are related by the Nernst-Einstein equation,

$$D_i = RT \mu_i, \quad 4.$$

where  $D_i$  is the diffusion coefficient,  $\mu_i$  is the mobility,  $R$  is the ideal gas constant, and  $T$  is the temperature.

Conductivity can be generalized to both ionic and electronic charge carrier transport. The measured ionic conductivity represents contributions from mobile cations and anions in the polymer, while the electronic conductivity is dominated by contributions from positive (holes) and negative (electrons) charge carriers in p- and n-type conducting polymers, respectively. The conductivity of a particular species,  $i$ , is given as

$$\sigma_i = p_i e |z_i| \mu_i, \quad 5.$$

where  $p_i$  is the ion concentration/charge carrier density,  $e$  is the charge of an electron,  $z_i$  is the integer charge, and  $\mu_i$  is the mobility.

When the application of an electric potential drives the transport of more than one charged species, it is useful to define the fraction of charge carried by each species. The fraction of total current carried by a single species,  $i$ , is the species transport number,

$$t_i = \frac{\sigma_i}{\sigma_{\text{total}}}, \quad 6.$$

**Table 1** Scaling dependencies of the overall diffusion coefficient and the transport number depending on the relative mobility (diffusion coefficient) of the mobile ion and mobile charge carrier (20)

Relative diffusion coefficient	Overall diffusion coefficient scaling	Transport number scaling
$D_X \gg D_e$	$D \cong D_e$	$t_X \cong 1, t_e \cong 0$
$D_X = D_e$	$D \cong D_e \cong D_X$	$t_X = (c_t - c_e)/(c_t - c_e^2)$ , $t_e = (1 - c_e)c_e/(c_t - c_e^2)$
$D_X \ll D_e$	$D \cong D_X$	$t_X \cong 0, t_e \cong 1$

$D_X$ ,  $D_e$ , and  $D$  are the ion diffusion coefficient, the charge carrier diffusion coefficient, and the overall diffusion coefficient, respectively.  $t_X$  is the transport number of the mobile ion, and  $t_e$  is the transport number of the mobile charge carrier.  $c_e$  is the concentration of the mobile charge carrier, and  $c_t$  is the combined concentration of the mobile charge carrier and mobile ion. Table adapted with permission from Reference 20; copyright 1989 American Chemical Society.

where  $t_i$  is the transport number,  $\sigma_i$  is the conductivity of species  $i$ , and  $\sigma_{\text{total}}$  is the sum of bulk conductivity that results from the sum of all  $\sigma_i$ .

In mixed conducting polymers, the mobility of all charged species may vary drastically, which affects the resultant diffusion coefficients of the system. A study of mixed conducting polymeric osmium perchlorate ion-exchange membranes analyzed the limiting cases in which (a) the diffusion coefficient of one species is much greater than the other and (b) diffusion of both species is equal (20). In this system, electrons are not delocalized but instead hop in a similar fashion to ions. For the case in which one species (either the ion or the electronic charge carrier) is more mobile than the other, the local field that results from the more mobile species drives the less mobile species to minimize the energy of the field. An important finding of this work is that in these limiting cases, the overall diffusion coefficient is proportional to the diffusion coefficient of the less mobile species. **Table 1** summarizes these findings. For the case in which the diffusion coefficients of the mobile species are equal, the overall diffusion coefficient is also the same. As expected, the species transport number is greater when the relative diffusion coefficient of the species is greater. When the diffusion coefficients are equal, the transport number scales nonlinearly according to the relative concentrations of both the mobile ion and electronic charge carrier.

Typically, the diffusion coefficient of the electronic charge carrier is much greater than that of ions in mixed conducting systems. For example, the diffusion coefficient for polarons in poly(3-hexylthiophene) (P3HT) ranges from  $10^{-5}$  to  $10^{-3}$   $\text{cm}^2/\text{s}$  [mobility of  $10^{-3}$  to  $10^{-1}$   $\text{cm}^2/(\text{V}\cdot\text{s})$ ], depending on the carrier concentration (23). The diffusion coefficient for perchlorate ( $\text{ClO}_4^-$ ) in P3HT is  $\sim 10^{-14}$   $\text{cm}^2/\text{s}$  (24). When solvent is added, the diffusion coefficient of  $\text{ClO}_4^-$  increases to values of  $10^{-12}$  to  $10^{-10}$   $\text{cm}^2/\text{s}$  (25). These order-of-magnitude differences in the diffusion coefficient between ions and electronic charge carriers indicate comparable differences in the timescales of transport; to a good approximation, these processes can be decoupled in time.

Although Fickian transport is used to describe the motion of charges in several materials classes, the assumptions inherent to Fickian diffusion are not applicable in mixed conductors. Fickian diffusion is typically well defined only in the dilute limit, at which interspecies interactions can be neglected. Recent work utilizing moving front experiments has provided evidence that ion transport in a conjugated polymer with glycolated side chains is non-Fickian and, in fact, reminiscent of ion transport in inorganic materials (26). As discussed in subsequent sections, charge-charge interactions are unavoidable at application-relevant ion concentrations (conductivity of  $\geq 10^{-3}$  S/cm) (22, 27).

## 2.2. Ionically Conducting Polymers

Ion conduction in polymer electrolytes is a hierarchical process impacted by both the mesoscale ( $\sim 10$ – $100$  nm) and molecular-scale ( $< 10$  nm) structure and dynamics of the electrolyte. At the

molecular scale, ionic transport involves an interplay of polymer segmental dynamics and ion-polymer solvation interactions, which simultaneously dissociate ions. These effects allow for long-range migration in response to an electric potential and act as frictional sources for ions, limiting their mobility on certain timescales. Transport at mesoscopic length scales is believed to require percolated regions of ion-solvating sites. Since ion-solvating sites are not fixed within the material, long-range transport depends on both the equilibrium ionic structure of the material and its fluctuation dynamics.

Ion transport in amorphous polymers is traditionally viewed as a liquid-like mechanism in which the local frictional environment dictates long-range ion transport (17, 28). Consequently, the temperature dependence of ionic conductivity correlates with measures of segmental mobility, such as the inverse of the segmental relaxation timescale,  $1/\tau_\alpha$  (4, 29, 30). As a result, ionic conductivity follows commonly known relationships for the temperature dependence of polymer dynamics such as the Vogel-Tammann-Fulcher (or equivalent Williams-Landau-Ferry) relationship (Equation 7) (31),

$$\sigma = \sigma_0(T) \exp\left(-\frac{B}{T - T_0}\right) \text{ for } T > T_g, \quad 7.$$

where the fitting parameter,  $\sigma_0$ , relates to the number of mobile ions;  $B$  relates to the activation energy associated with segmental motion; and  $T_0$  is a reference temperature corresponding to the temperature of zero configurational entropy and typically takes on universal values ( $T_0 \cong T_g - 50$  K, where  $T_g$  is the glass transition temperature) (31). It is common either to treat  $\sigma_0$  as a temperature-independent constant or to assign it to scale with  $T^{-1/2}$  dependence. **Figure 1a** depicts how polymer segmental motion gives rise to pathways for ion transport. Strategies to increase ionic conductivity of polymeric electrolytes include adding more salt, which increases the number of charge carriers (32); increasing the dielectric constant, which enhances salt dissociation (33); and increasing segmental mobility (lowering  $T_g$ ) (4).

The ionic conductivity of polymer electrolytes often far exceeds expectations from the liquid-like mechanism of ionic conduction in glassy and crystalline regions, suggesting an alternative transport mechanism in which ion motion is decoupled from polymer relaxation (34). In glassy

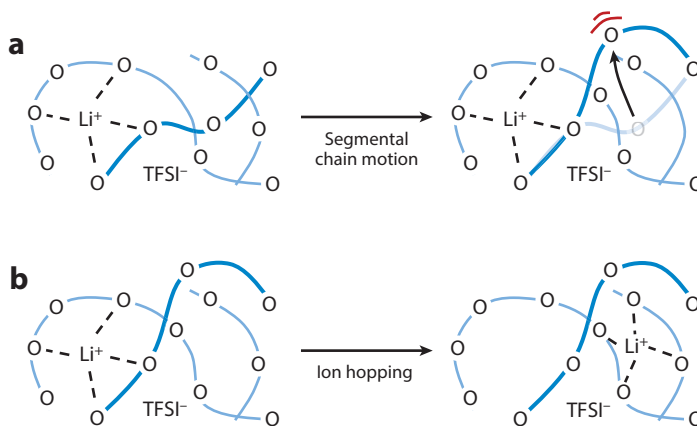


**Figure 1**

Mechanisms of ion conduction. (a) Ion transport is fostered by electrostatic interactions with electron-withdrawing moieties on the polymer side chain. As segments of the polymer chain move, free-volume sites become available. (b) When free-volume sites are nearby, ions can hop from one site to another. Abbreviation: TFSI, bis(trifluoromethanesulfonyl)imide.

or crystalline regions of the electrolyte, the temperature dependence of ion motion commonly follows an Arrhenius form (Equation 8) (16, 35),

$$\sigma_0 = \sigma_0(T) \exp\left(-\frac{E_a}{k_B T}\right), \quad 8.$$

where the activation energy ( $E_a$ ) is now associated with ion hopping rather than segmental motion. **Figure 1b** depicts how ions might hop via an Arrhenius hopping mechanism. For ordered phases, ions may hop between free-volume sites within the polymer matrix.

Polymeric mixed conductors are often semicrystalline; the bulk ionic conductivity is a weighted sum of contributions to ionic conductivity in both the amorphous and crystalline phases. Below  $T_g$ , segmental chain motion is limited and ions are transported by hopping in both phases, as described by Equation 8. Because conductivity is greater in the amorphous phase, the design rule for enhancing ionic conductivity in solely ion-transporting polymers is usually to reduce or remove the crystalline fraction. In mixed conducting polymers, the crystalline regions are helpful for conduction of electronic charge carriers. As a result, ion conduction in mixed conducting polymers is frequently dominated by transport through amorphous domains. Above  $T_g$ , motion of polymer chain segments creates free-volume sites for ion motion, providing another contribution to ion conduction, as described by Equation 7. However, ion hopping can still occur in both phases. **Figure 2** shows the various temperature regimes in which significant differences in the mechanism of ionic conduction are observed and how the bulk ionic conductivity might arise from individual mechanistic contributions. An important distinction between ion conduction in

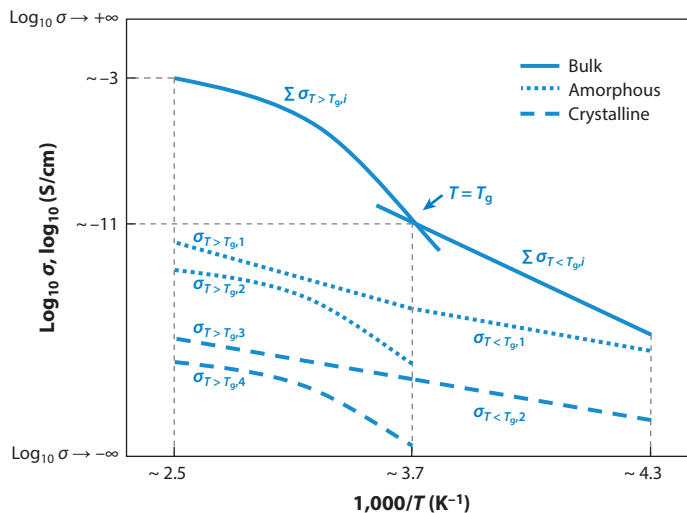


**Figure 2**

An Arrhenius plot of temperature dependence of ionic conductivity in polymers. Approximate values are estimated from ionic conductivity in representative polymeric ionic liquids (27). In semicrystalline polymers, the bulk ionic conductivity is a sum of individual contributions in both the crystalline and amorphous phases. At temperatures below the glass transition temperature,  $T_g$ , ion hopping in both the amorphous ( $\sigma_{T < T_g,1}$ ) and crystalline phases ( $\sigma_{T < T_g,2}$ ) is the dominant mechanism of ion transport. At temperatures above  $T_g$ , ion transport mediated by segmental chain motion ( $\sigma_{T > T_g,2}$ ,  $\sigma_{T > T_g,4}$ ), along with ion hopping ( $\sigma_{T > T_g,1}$ ,  $\sigma_{T > T_g,3}$ ), can take place in both phases. Log-linear contributions in the Arrhenius plot describe ion hopping via the Arrhenius equation, while nonlinear contributions describe segmental chain motion-mediated transport via the Vogel-Tammann-Fulcher equation. Figure adapted with permission from Reference 27; copyright 2020 American Chemical Society.

solely ion-conducting polymers and in mixed conducting polymers is that there are at least two energy barriers to ion motion in mixed conducting polymers. Solely ion-conducting systems are mostly amorphous, and the primary mechanism is related to ion motion in the amorphous phase. Because mixed conducting polymers are usually semicrystalline, energy barriers for both ion hopping and segmental motion-mediated transport contribute to ionic conductivity in the crystalline and amorphous phases, respectively.

Molecular-scale interactions between the polymer and mobile ion also contribute to ion transport. Because cations are typically the mobile ion of interest for many applications, strategies to increase the dielectric constant and introduce electron-rich moieties facilitate transport of cations in addition to segmental motion (36). However, stronger interactions can detrimentally affect the relaxation processes of polymers (37), potentially due to the change in chain dimensions at high salt concentration (38). This effect likely contributes to the maximum ionic conductivity with salt concentration observed in many ion-conducting systems (39). Pioneering simulations and experimental work have demonstrated aggregate structures ranging from isolated, spherical aggregates to percolated, stringy aggregates obtained through modifications in polymer repeat structure, ion identity, and polymer architecture (40). Materials with ions tethered directly along the backbone (ionenes) can display highly ordered ion structures, resulting in materials segregated into ion-rich domains (12) that display well-defined long-range order into unit cells with lattice parameters of  $\sim 3\text{--}7$  nm below an order-disorder temperature (41, 42).

Analogously, mesoscale segregation of block copolymers and polymer blends has been leveraged to generate materials with percolated ionically conductive domains on larger length scales (10–100 nm) (43, 44). Though modification of an ion-conducting material such as poly(ethylene oxide) (PEO) with an insulating domain is generally regarded to be detrimental to ionic conduction, insulating domains are often incorporated to impart structural rigidity. The effect of these insulating domains can range from a minimal impact on performance in the case of percolating morphologies to a dramatic insulating character in nonpercolating morphologies (45–47). These examples serve to demonstrate the importance of continuous connection of ion-conducting domains across all device length and timescales, signifying the hierarchical nature of ion conduction.

### 2.3. Electronically Conducting Polymers

In purely electron-conducting polymers, transport occurs both through delocalized  $\pi$ -orbitals along one chain and by hopping between chains if sufficient  $\pi$ - $\pi$  overlap exists (48). Because most conjugated polymers are semicrystalline, heterogenous electronic conduction between the amorphous and crystalline domains of the polymer results in complex behavior in which the effects of separate mechanisms, such as charge transport along a polymer chain or charge hopping from one chain to another, are difficult to deconvolute. Similar to ion-conducting polymers, molecular-scale interactions and morphology have a profound effect on the electrical properties of semiconducting polymers (5).

To increase the electrical conductivity of polymers, carriers are introduced into the material through doping. Doping involves oxidation (reduction) of the backbone through an extrinsic molecule or an electrode, which forms a radical/hole (radical/electron) pair along the polymer backbone (49). In contrast to inorganic conductors, the charge-balancing ion must reside near the backbone charge, a phenomenon that has important implications on the double-layer capacitance, as discussed in Section 3.3. One central question in doping polymeric semiconductors is how the presence of these ions affects other material properties of the polymer, which impacts the resulting transport behavior.

The mobility of electronic charge carriers is highest in the crystalline regions of the system. The specific transport mechanisms are typically identified through temperature-dependent

scaling behavior. The electronic mobility or electrical conductivity typically follows a power law ( $\sigma \sim T^{-a}$ ) or a stretched exponential ( $\sigma \sim \exp[-T^{-b}]$ ) relationship with respect to temperature. Common models observed in temperature-dependent measurements of semiconducting polymers include variable range hopping ( $b = 1/4 - 1/2$ ), nearest neighbor ( $b = 1$ ), and band transport ( $a \cong -1$ ) (15, 50). The heterogenous morphology of semiconducting polymers complicates the identification of a primary transport mechanism at a given temperature since the mechanism may spatially vary with the molecular-scale structure. Convoluting effects, such as changes in electronic charge carrier densities, can be monitored via thermopower measurements, which are related to the electronic density of states (51, 52).

Although morphology is important for mixed conduction, the process of crystallization is difficult to control in semiconducting polymers. The tendency for crystallization in polymers depends on the specific chemistry, including the regioregularity of the pendant groups along the polymer backbone; the introduction of other species, such as dopants; and the effects of postprocessing, such as thermal annealing (53, 54). The conjugated backbone and ring-like structures common in semiconducting and conducting polymers tend to stiffen the polymer backbone, which increases the propensity to form liquid crystalline phases and crystallize upon casting. As a result, mixed conducting polymer systems are often semicrystalline, and few studies to date have reported on electronic conduction at temperatures above  $T_m$ . **Figure 3** shows how the molecular structure in ordered P3HT gives rise to the observed microscopic structure and how the alignment of polymer chains may lead to local anisotropy of electronic conductivity.

A holistic description of molecular-scale interactions between charged species and electronically conducting polymers is complicated due to the fact that the electron (or hole) resides on the polymer itself, while the counterion resides in proximity to the backbone with a potentially different energetic landscape (55, 56). Theoretical calculations can explore these effects separately. Recent simulations of P3HT oligomers using density functional theory compared the  $\pi$ -stacking distance of the oligomers with and without a polaronic charge on the backbone (57). The calculations determined that even in the absence of dopant counterions, the presence of a positive charge decreases the  $\pi$ -stacking distance by 0.02–0.08 Å, depending on the number of repeat units analyzed. The model suggests that relaxation of the polaron between multiple chains leads to attractive forces between units, resulting in a decrease of the  $\pi$ -stacking distance. These results are in agreement with operando X-ray scattering measurements of electrochemically doped P3HT (56, 58) but do not rationalize the additional impact of the increasing concentration of counterions present within the polymer film.

An understanding of how interactions between the charge carrier on the polymer and its counterion affect the electronic mobility is still evolving. The counterions typically reside in the amorphous regions of the polymer due to the increased free volume of these domains or within the side chain region of polymeric crystallites. The low dielectric constant of most conjugated polymers (typically synthesized with alkyl side chains) can lead to localization of the polaron on the polymeric backbone since the Coulombic interactions with the counterion cannot be effectively screened. These deleterious interactions have been mitigated by introducing more polar side chains, causing electrostatic interactions to be screened (59, 60), or by using sterically bulky dopants, which generally have shallower Coulombic potential wells (61). These design principles may serve to improve other aspects of transport specific for mixed conduction, such as improving ion uptake in aqueous environments (62).

The degree of crystallinity and connectivity between neighboring crystallites within semicrystalline polymers at the mesoscale (50–500 nm) largely governs the resulting electronic conductivity. The electronic mobility generally scales with the degree of crystallinity, since energetic trap states are induced by conformational disorder within the amorphous domains of the polymer.

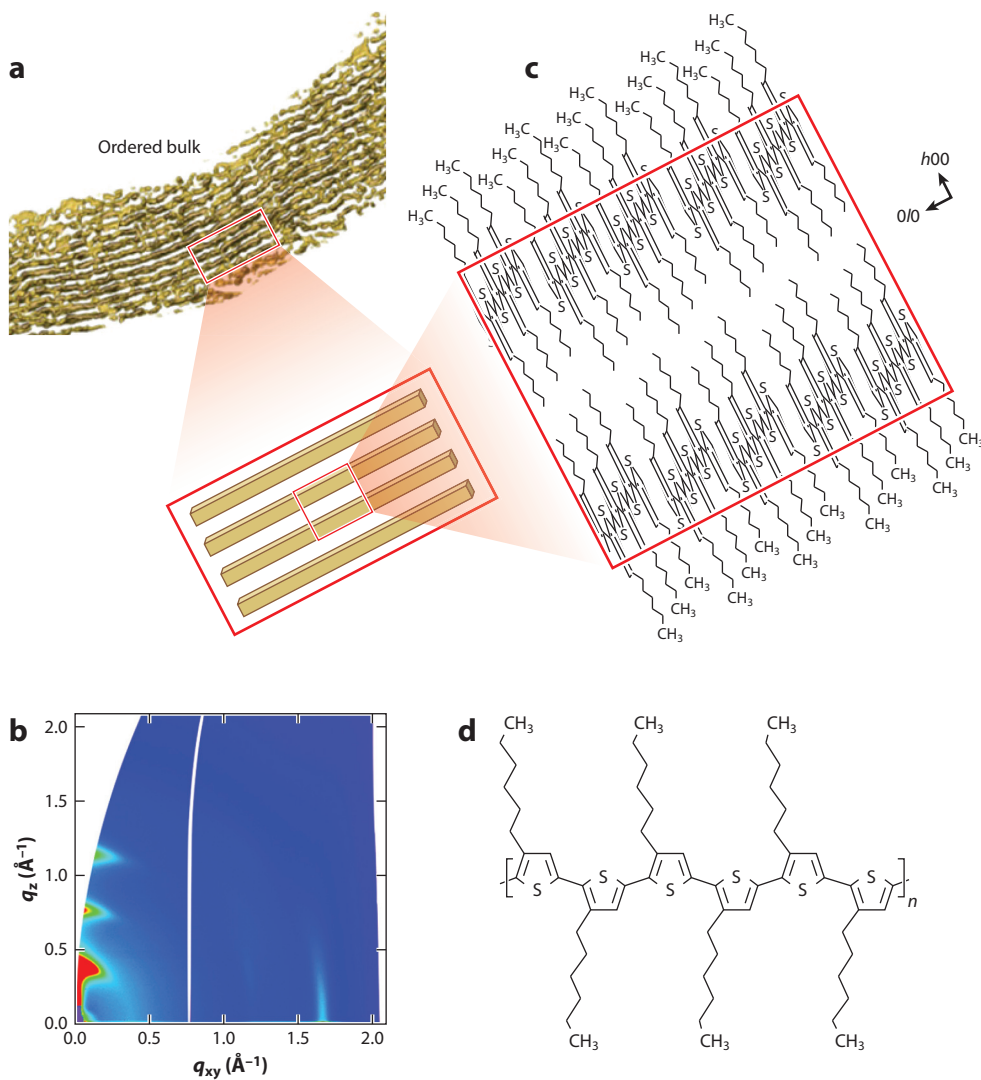


**Figure 3**

Structural orientation of poly(3-hexylthiophene) (P3HT) in a crystallite. (a) A 3D reconstruction of ordered domain nanostructure from an electron micrograph is shown (98). In this image, the polymer chain is viewed on its edge, and alkyl side chains extend between backbone stacks and are oriented orthogonally to the principal axis of the polymer. (b) A grazing incidence wide-angle X-ray scattering (GIWAXS) pattern is shown for ordered P3HT. The signal near the  $q_z$  direction corresponds to periodic stacking between adjacent polymer segments separated by alkyl side chains ( $b00$ ), while the signal along the  $q_{xy}$  direction corresponds to the  $\pi$ - $\pi$  stacking distance between adjacent polymer backbones ( $0/0$ ). (c) The inset shows the projected ordering as a stack of high-aspect-ratio rectangular prisms. Further magnification shows the molecular structure of P3HT oriented to match the nanostructure of ordered P3HT observed in panel a. Vectors showing the  $b00$  and  $0/0$  direction are labeled to aid in comparison to the GIWAXS pattern shown in panel b. (d) The molecular structure of P3HT is shown for comparison to the tomography image-aligned molecular structure shown in panel c. Panels a, c, and d adapted with permission from Reference 98; copyright 2014 American Chemical Society. Panel b adapted with permission from Reference 64; copyright 2019 Wiley-VCH Verlag.

Strategies such as altering the casting solvent or the backbone regioregularity were found to influence the fraction of aggregated regions in the film and their free exciton bandwidth, which scaled with the electrical conductivity (63, 64). The distance over which polymeric backbones retain alignment with one another, defined as the orientation correlation length (OCL) (65), also influences the electrical properties of polymers. In contrast to the crystallites themselves, which are typically  $\sim 10$  nm in size, the length scale over which they are connected is a strong determinant of the electronic conductivity even at similar carrier concentrations. The OCLs of pristine P3HT are typically below 50 nm (64) but can reach up to 350 nm in liquid crystalline semiconductors such as poly[2,5-bis(3-tetradecylthiophen-2-yl)thieno[3,2-*b*]thiophene] (66). Recent studies found that the doping method can degrade this long-range order, influencing the maximum achievable electrical conductivity (55, 63). These results suggest that retaining the alignment between ordered domains when ions are present is critical for electronic and mixed conduction.

Tie chains, molecules that connect ordered regions, are also necessary to create a percolated pathway for electronic charge carriers. Tie chains must possess a sufficient contour length to connect two neighboring crystallites, which requires a minimum degree of polymerization. In homopolymers, a discontinuous increase in electronic mobility typically occurs at  $\sim 12,000$ – $15,000$  g/mol, or about 70–90 repeat units for P3HT (5). The same effect can be achieved through mixing small amounts of a high-molecular-weight polymer with the same polymer of lower molecular weight; analysis of P3HT blends found that only  $10^{-3}$  of all chains need to act as tie chains for a percolated network to form, even when the degree of polymerization of the majority phase is as small as 30 repeat units (67, 68).

### 3. IONIC, ELECTRONIC, AND MIXED CONDUCTION FIGURES OF MERIT

#### 3.1. Ionic Transport

While the total ionic conductivity is the most commonly reported metric of ionic transport in polymer electrolytes, actual electrolyte performance in energy storage and conversion devices heavily depends on a more comprehensive view of ion conduction. For example, in lithium-ion batteries, the ionic current carried by  $\text{Li}^+$  ions is of primary interest and counterion motion can be detrimental to cell performance. Consequently, the transport number is an important parameter to approximate the fraction of the total current carried by the ion of interest (see Equation 6) (69).

A quantity known as the Haven ratio (Equation 9) is used to characterize the ratio of the measured ionic conductivity and the ionic conductivity reproduced from the Nernst-Einstein relation (Equation 4):

$$H = \frac{\sigma_{\text{NE}}}{\sigma_{\text{electrochem}}} = \frac{\sum_i n_i z_i^2 D_i}{kT \sigma_{\text{electrochem}}}. \quad 9.$$

In Equation 9,  $H$  is the Haven ratio,  $\sigma_{\text{NE}}$  is the Nernst-Einstein conductivity,  $\sigma_{\text{electrochem}}$  is the electrochemically determined conductivity,  $n_i$  is the number of charge carriers  $i$ ,  $z_i$  is the integer charge of the charge carrier,  $D_i$  is the diffusion coefficient,  $k$  is the Boltzmann constant, and  $T$  is the temperature.

A discussion of methods to determine the Nernst-Einstein and electrochemically determined conductivity is provided in Section 3.4. The Haven ratio often takes on a value of less than unity for ionic liquids or molten salts (70) but can take on values greater than unity for superionic conductors (71). In some concentrated polymer electrolytes, Haven ratios of near unity are observed, but authors should take care to note that deviations from the Nernst-Einstein relation are likely to arise, particularly at high ionic strengths or in the presence of crystalline regimes. As such, Haven

ratio values far from unity are indicative of intermolecular interactions that lead to differences between ionic diffusivity and charge diffusivity, such as ion aggregation.

### 3.2. Electronic Transport

The electrical conductivity,  $\sigma$ , combines the concentration, mobility, and charge of the mobile species (Equation 5). For doped polymeric semiconductors, the electrical conductivity is the most commonly reported transport parameter and represents an average of all electronic conduction mechanisms that occur within the material. The highest reported values for doped polymers are between  $10^4$  and  $10^5$  S/cm at ambient temperatures (72, 73). The electrical conductivity at a single temperature, however, does not reveal the complex relationship between the variables it depends on (14, 51).

Electronic mobility,  $\mu$ , provides a metric to understand how carrier concentration influences transport. In lightly doped polymeric semiconductors (charge carrier density of  $<10^{20}$  cm $^{-3}$ ) (23), many of the carriers are energetically trapped, leading to a carrier mobility of  $\sim 10^{-3}$  cm $^2$ /(V·s). For comparison, the ionic mobility of ClO $_4^-$  in P3HT is on the order of  $10^{-14}$  cm $^2$ /s (24). Adding more charge carriers leads to a superlinear increase in the electronic mobility, reaching up to  $\sim 0.1$ – $1$  cm $^2$ /(V·s) for some of the highest-performing semiconducting polymers. This superlinear trend is unique to polymeric semiconductors and has been rationalized by several mechanisms in recent literature (51, 74). Thus, the charge density is a critical independent variable of transport phenomena in electronic conduction and is necessary to quantify for electronic as well as ionic and mixed conduction.

### 3.3. Mixed Conducting Systems

Performance metrics for mixed conducting polymers vary widely based on application; for example, when mixed conductors are applied to biological sensors and actuators, a fast response time is an important figure of merit. In electrochromic devices, the contrast ratio of color and brightness may be a better metric for performance. The application of polymeric mixed conductors in ion pumps means that precise control over ion flux is crucial, while sensing applications depend on changes in electron or ion flux in response to external stimuli. Because of the range of potential applications, a single figure of merit to describe the performance of mixed conductors has not been established.

The increasing utility of studying polymeric charge transport through organic electrochemical transistors (OECTs) (Figure 5a), along with uncertainties in individual measurements of ionic and electronic mobility, has bolstered the use of the transconductance as a figure of merit for mixed conduction. Since transistors are used as electrical amplifiers, the transconductance quantifies how much current is gained in the active layer for a given change in the gate voltage. Because  $dI/dV_g$  depends on the channel width ( $W$ ), length ( $L$ ), and thickness ( $d$ ), the transconductance is also a means to normalize across device dimensions. Several factors contribute to the device transconductance ( $g_m$ ) according to Equation 10,

$$g_m = (Wd/L)\mu C^*(V_{th} - V_g), \quad 10.$$

where  $\mu$  is the electronic mobility,  $C^*$  is the volumetric capacitance of the active layer,  $V_{th}$  is the threshold voltage, and  $V_g$  is the gate voltage.

While transconductance can be used to describe the performance of transistors, capacitance is a more generalizable figure of merit that can be used to benchmark performance for all mixed conducting devices. The chemical capacitance, defined by the change in chemical

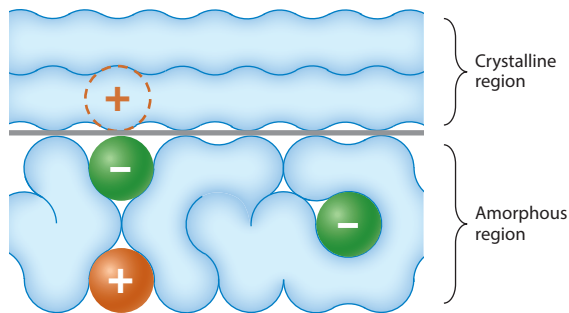


**Figure 4**

A capacitance arising from a crystalline-amorphous interface in a mixed conducting polymer. In p-type mixed conductors, electron transfer between dopant anions (*green*) in the amorphous regions and polymer backbones (*blue*) in the crystalline regions generates charge carriers (polarons, outlined in *orange*). The interaction between multiple charged species can lead to charged complexes, such as a hole-anion-cation-anion complex.

potential of the material for a change in carrier concentration (75), ultimately mediates other application-specific figures of merit, such as the contrast ratio in electrochromics (76) and the flux in ion pumps and membranes (77). Chemical capacitance is an extensive quantity, and thus proportional to the volume of the sample, and describes both a redox reaction and diffusion of the external species into the surface and bulk. Because all mixed conductors require this two-step mechanism, chemical capacitance may be one potential route for a generalized performance metric in mixed conductors.

The total capacitance also includes contributions from the electrical double-layer (EDL) capacitance, which arises from the accumulation of charges at the interface between an electrode and electrolyte material. In an electrochemical cell, a metal electrode is primarily responsible for electronic conduction, whereas the electrolyte is primarily responsible for ionic conduction, and the EDL is developed at their interface. Locally, the coupling between ions and charge carriers can be described by analogy between metal electrodes and crystalline regions and between electrolytes and amorphous regions. **Figure 4** shows how a positively charged hole might be balanced not only by a single anion molecule, but also by electrostatic complexes, such as a hole-anion-cation-anion complex at the ordered-disordered interface. Because electrical fields and associated potential gradients couple ions and electronic charge carriers, these distinct transport processes may be approximated as decoupled in time, but not in space.

It is apparent that EDL charging depends on both electronic and ionic species distributions within the bulk. Specifically, the applied potential in organic electronic devices drives ions toward ordered-disordered interfaces where charge carriers are induced and coupled with nearby dopant ions. Local electric fields arise from this separation of charge and can be accounted for in the boundary conditions necessary to solve Equations 1 and 2.

Lastly, an important feature that is not often considered in OECTs is the dynamics of ion transport. Since ion transport occurs on observable timescales ( $10^{-3}$  s), limitations in ion transport may significantly affect device performance and are observable through the transconductance (78–80). The rate at which output and transfer characteristics (**Figure 5b**) are obtained is not often reported as the field of OECTs continues to expand, but understanding the kinetic component will be critical for rational design of high-performance polymeric mixed conductors (81, 82).

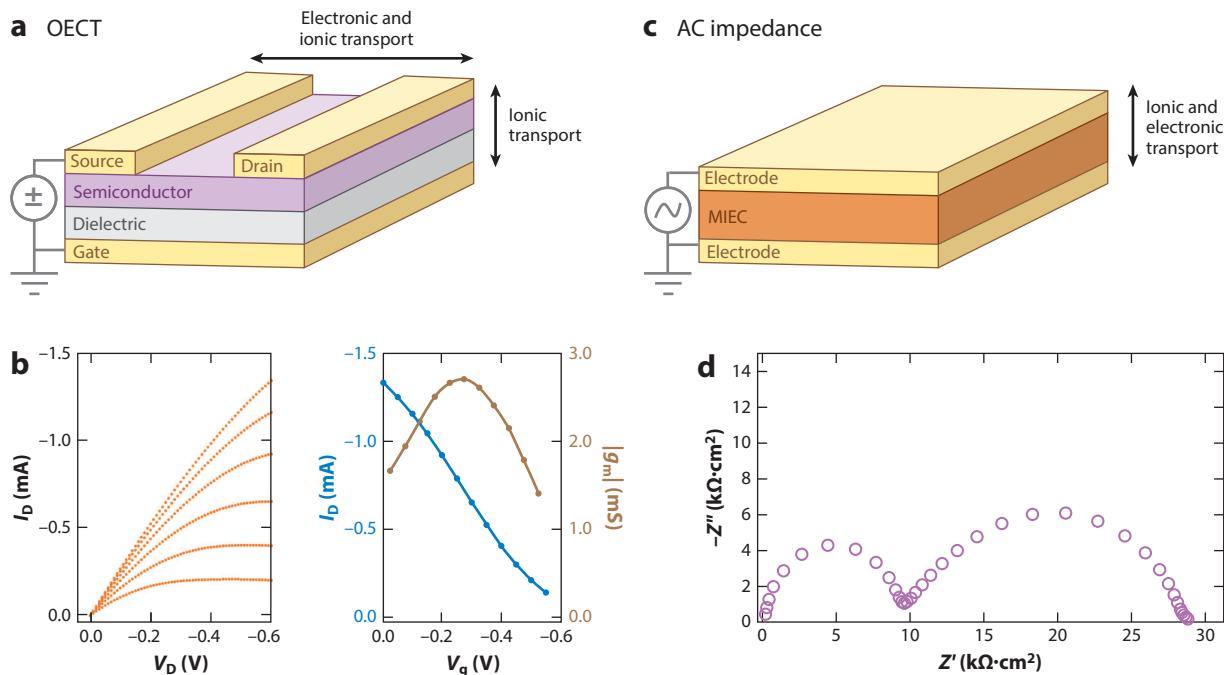


**Figure 5**

Two common platforms to characterize ionic and electronic transport of polymeric semiconductors are the organic electrochemical transistor and symmetric cell. (a) Ions and electrons travel in orthogonal directions within organic electrochemical transistors, which decouples ionic and electronic conduction. (b) Output and transfer curves from organic electrochemical transistor operation yield information about the performance of the mixed conducting device (99). (c) Using AC impedance, both charge carriers travel in the same direction. (d) A Nyquist plot of the frequency-dependent response is one straightforward visualization of the contributions of electronic and ionic motion (87). The presence of multiple semicircles in the Nyquist plot indicates motion of more than one chemical species in the sample. Abbreviations: MIEC, mixed ionic–electronic conductor; OECT, organic electrochemical transistor. Panel *b* adapted with permission from Reference 99; copyright 2013 Springer Nature. Panel *d* adapted with permission from Reference 87; copyright 2012 American Chemical Society.

### 3.4. Measurement Methods

The complex impedance measured by electrochemical impedance spectroscopy (EIS), or AC impedance, is widely used to deconvolute individual contributions of ionic and electronic transport in mixed conductors (Figure 5c). These contributions are determined through construction of an equivalent circuit model to fit the impedance data (Figure 5d). Generally, the equivalent circuit is designed with physical phenomena in mind to connect the circuit elements with the physical behavior in the sample; however, the complex behavior of mixed conductors can create complications that go beyond simplistic circuit elements. An important advantage of EIS is its ability to deconvolute processes occurring on widely divergent timescales.

The Bruce–Vincent method is a cell-based method frequently employed to determine the species-dependent transport number of ionic species (12). This method employs a symmetric electrochemical cell (Figure 5c) and can relate the steady-state DC voltage of the cell to the transport of a specific species under dilute conditions. Consequently, this method does not give a true transport number under conditions relevant for many applications. The dilute approximation generally applies only at low ionic strengths (<0.01), which is much less than the ionic strength typical for an electrolyte (18). Despite the inability to extract relevant transport numbers under common

conditions, the ease of implementation has resulted in wide propagation of this method, and it has become standard in the field of ionically conducting polymers. Therefore, the results of this experiment are important for benchmarking purposes and to compare between materials systems. Recent developments in cell-based methods may allow better estimation in concentrated solutions, including direct measurement of the concentration gradient along the transport direction and analysis based on a concentrated solution theory (83).

An alternative family of techniques to examine ion-specific transport utilizes measurements of ion self-diffusion constants, and their contribution to conductivity is also calculated based upon the assumptions of the Nernst-Einstein equation. Techniques such as pulsed-field gradient nuclear magnetic resonance spectroscopy can measure the self-diffusion constants of ions (84, 85). Neglecting intermolecular interactions, the ionic conductivity contributions from individual species are directly related to this constant, their concentration, and valency, allowing for facile computation of their contribution to the total conductivity. However, experimental reconstructions of the net ionic conductivity based on these results often fail to reproduce the measured ionic conductivity, as indicated by the Haven ratio (Equation 9).

As previously mentioned, OEETs are a unique platform to study the principles of mixed conduction relevant to many applications of ion/electron conductors. OEETs contain the same components as field-effect transistors and typically adopt similar geometries (**Figure 5a**). They are distinguished by their use of gate insulators that contain cations and anions that infiltrate the semiconducting layer upon application of a gate bias. Synthetically tethering the cation or anion species of the gate dielectric facilitates control over ion diffusion into the semiconductor, preventing unwanted ion pair infiltration into the material (23, 86). As a result, the semiconductor can sustain charge throughout the bulk of the layer via ionic motion. OEETs also provide experimental control over the carrier density of ions and electrons critical in rationalizing the impact of ions on the mobility, morphology, and electronic structure of the semiconductor (15, 51, 56).

## 4. EMERGING AREAS IN MIXED CONDUCTION

Separate application of ionically and electronically conducting polymers has led to an imperfect understanding of mixed conducting materials. Studies purely on one-component charge transport conclude that the material properties beneficial for one type of transport are detrimental to the other. Studies in polymeric mixed conductors have shown that this idea may not be the case, which is counterintuitive to our current understanding (11, 87). This section details the subfields of mixed conductors that require more investigation.

### 4.1. Dynamic Structural and Morphological Disorder

The previous sections have highlighted the importance of morphology for all forms of transport in polymeric semiconductors. Consequently, the structural changes of semiconducting polymers upon ion incorporation are key to understanding transport in these materials (88). It is of utmost importance then to understand how morphology evolves as more ionic species are added to the material. For example, interactions between electrically and ionically conducting domains can lead to structural rearrangement, contributing to an increase in mixed conduction. This effect was seen in P3HT:PEO block copolymers doped with lithium bis(trifluoromethanesulfonyl)imide salt (87). Upon adding salt to the copolymer, both the electrical and ionic conductivity increased. While the increase in ionic conductivity is expected, the increase in electrical conductivity implies a structural rearrangement leading to improved electronic charge transport. Structural rearrangements due to solvent treatments also improve the mixed conductivity of PEDOT:PSS and poly[6-(thiophene-3-yl)hexane-1-sulfonate] tetrabutylammonium (89).

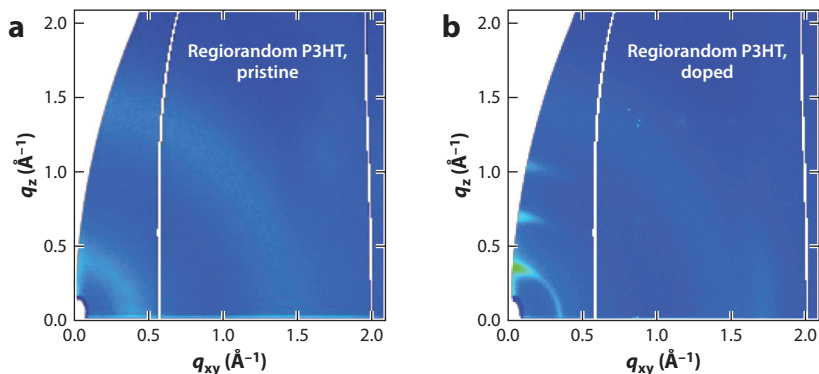


**Figure 6**

Grazing incidence wide-angle X-ray scattering measurements of poly(3-hexylthiophene) (P3HT) indicate doping-induced reversible formation of crystallites (64). (a) Broad peaks are observed for regiorandom P3HT, while (b) clear features near the  $q_z$  axis appear upon doping with 2,3,5,6-tetrafluoro-7,7,8,8-tetracyanoquinodimethane. Figure adapted with permission from Reference 64; copyright 2019 Wiley-VCH Verlag.

While many studies show an increasing degree of disorder upon adding salts or dopants in semicrystalline materials, few studies have probed the morphological effects of doping polymers that are already amorphous. Regiorandom P3HT is primarily amorphous on its own, but it reversibly orders and returns to its amorphous state upon the addition and removal of the dopant 2,3,5,6-tetrafluoro-7,7,8,8-tetracyanoquinodimethane (**Figure 6**) (64). These results suggest that the amorphous regions of conjugated polymers may be more structured than previously suggested and that a rigid amorphous phase may play a role in electronic conduction (90). Since morphology is critical to the performance metrics of mixed conductors, exploring these ideas will have critical utility for large-scale implementation of these systems.

## 4.2. Dielectric Environment

The dielectric environment controls salt dissolution and therefore directly impacts ionic concentration and conductivity, but the impact of the dielectric constant on electronic transport of mixed conductors is less clear. Though previous work suggests that increases in dopant/polaron distance do not translate to higher electronic conductivity (91), it has been recently demonstrated that the formation of dianions within highly polar thienothiophene-based polymers with ethylene-oxide side chains leads to superior electrical performance (92). This behavior may be a result of the increased dielectric constant of the polar side chains stabilizing the dianion, leading to fewer ionic charges per electronic charge. Charge-stabilizing effects of an increased dielectric constant were also observed in a 3,4-ethylenedioxythiophene-based polymer in which oligoether side chains enhanced the solubility of the polymer in several solvents, even in its charged state (93). Further investigation into how charge screening impacts carrier mobility will lead to crucial insights for designing polymeric mixed conductors both at the molecular level and at the mesoscale.

## 4.3. Mechanical Properties

The enhancement of the transport performance of mixed conductors is often accompanied by trade-offs in mechanical performance, which presents a challenge due to the demanding mechanical requirements for many applications of mixed conductors. Studies exploring the effect of strain

on the electronic mobility of polymeric semiconductors typically show consistent or even improved electronic mobility in the direction of strain due to the alignment of polymeric backbones (94, 95). This effect is usually coupled with a decrease in carrier mobility perpendicular to the strain direction. Similarly, ionic conductivity has been observed to increase as a result of increased strain through in situ studies, in which through-plane and in-plane conductivity increases linearly with deformation of 200- $\mu\text{m}$  PEO/LiClO<sub>4</sub> electrolyte films (96). Models to rationalize the effects of strain on the output characteristics of OECTs are also in development (97), which can elucidate fundamental relationships between conduction and mechanics of mixed conductors and establish practical boundaries for long-term operation. As with all performance metrics of mixed conducting polymers, the temperature dependence of the mechanical behavior of mixed conductors is crucial to deconvolute the elastic and viscous response to an applied strain, which can also evolve as a function of salt concentration. Connecting the fundamental relationships between conduction and mechanics of mixed conductors will further elucidate their behavior and establish practical limitations for long-term operation.

## 5. CONCLUSIONS

The field of polymeric mixed conductors requires an interdisciplinary perspective that combines knowledge of electronic and ionic transport with principles distinct to mixed conduction. The semicrystalline structure of mixed conducting polymers, containing percolated pathways for conduction of both ions and electrons, represents a clear design constraint for the morphology of mixed conductors; however, clear relationships between the morphology and various figures of merit for mixed conduction have yet to be elucidated. Expanding the structure-property relationships between these figures of merit and the percent crystallinity of polymers, which affects the capacitive component between ions and electrons in the material, has significant potential to create a unifying model for practical implementation of mixed conducting systems. This integrated picture is the ultimate path forward in designing polymeric materials to meet the demand of applications that require mixed conduction. Knowledge from synthetic chemistry, electrochemistry, and solid-state physics informs the rational design and processing required for the multitude of applications for mixed conducting materials. The principles developed in the organic electronics and polymer electrolyte communities will be helpful in guiding this field, but some relationships distinct to mixed conduction have yet to be fully realized.

## DISCLOSURE STATEMENT

The authors are not aware of any affiliations, memberships, funding, or financial holdings that might be perceived as affecting the objectivity of this review.

## ACKNOWLEDGMENTS

E.M.T. acknowledges support for work on ionic and electronic interactions in semiconducting polymers from the Department of Energy, Office of Basic Energy Sciences, under grant DE-SC0016390 and from a National Science Foundation Graduate Fellowship (DGE-1650114). S.D.J. gratefully acknowledges support from the Materials Research and Engineering Centers program of the National Science Foundation under award DMR 1720256 for work on ionic conduction. P.H.N. acknowledges support from the U.S. Army Research Office and accomplished under cooperative agreement W911NF-19-2-0026 for the Institute for Collaborative Biotechnologies for work on aqueous mixed conduction.

## LITERATURE CITED

1. Onorato JW, Luscombe CK. 2019. Morphological effects on polymeric mixed ionic/electronic conductors. *Mol. Syst. Des. Eng.* 4(2):310–24
2. Paulsen BD, Tybrandt K, Stavrinidou E, Rivnay J. 2020. Organic mixed ionic-electronic conductors. *Nat. Mater.* 19(1):13–26
3. Inal S, Rivnay J, Suiu A-O, Malliaras GG, McCulloch I. 2018. Conjugated polymers in bioelectronics. *Acc. Chem. Res.* 51(6):1368–76
4. Miyamoto T, Shibayama K. 1973. Free-volume model for ionic conductivity in polymers. *J. Appl. Phys.* 44(12):5372–76
5. Noriega R, Rivnay J, Vandewal K, Koch FPV, Stingelin N, et al. 2013. A general relationship between disorder, aggregation and charge transport in conjugated polymers. *Nat. Mater.* 12(11):1038–44
6. Chang WB, Fang H, Liu J, Evans CM, Russ B, et al. 2016. Electrochemical effects in thermoelectric polymers. *ACS Macro Lett.* 5(4):455–59
7. Patel SN, Javier AE, Balsara NP. 2013. Electrochemically oxidized electronic and ionic conducting nanostructured block copolymers for lithium battery electrodes. *ACS Nano* 7(7):6056–68
8. Dong BX, Liu Z, Misra M, Strzalka J, Niklas J, et al. 2019. Structure control of a  $\pi$ -conjugated oligothiophene-based liquid crystal for enhanced mixed ion/electron transport characteristics. *ACS Nano* 13(7):7665–75
9. Stavrinidou E, Winther-Jensen O, Shekibi BS, Armel V, Rivnay J, et al. 2014. Engineering hydrophilic conducting composites with enhanced ion mobility. *Phys. Chem. Chem. Phys.* 16(6):2275–79
10. Lai C-H, Ashby DS, Lin TC, Lau J, Dawson A, et al. 2018. Application of poly(3-hexylthiophene-2,5-diyl) as a protective coating for high rate cathode materials. *Chem. Mater.* 30(8):2589–99
11. Das P, Zayat B, Wei Q, Salamat CZ, Magdău I-B, et al. 2020. Dihexyl-substituted poly(3,4-propylenedioxythiophene) as a dual ionic and electronic conductive cathode binder for lithium-ion batteries. *Chem. Mater.* 32(21):9176–89
12. Evans CM, Bridges CR, Sanoja GE, Bartels J, Segalman RA. 2016. Role of tethered ion placement on polymerized ionic liquid structure and conductivity: pendant versus backbone charge placement. *ACS Macro Lett.* 5(8):925–30
13. Kang K, Watanabe S, Broch K, Sepe A, Brown A, et al. 2016. 2D coherent charge transport in highly ordered conducting polymers doped by solid state diffusion. *Nat. Mater.* 15(8):896–902
14. Arkhipov VI, Heremans P, Emelianova EV, Bässler H. 2005. Effect of doping on the density-of-states distribution and carrier hopping in disordered organic semiconductors. *Phys. Rev. B* 71(4):045214
15. Wang S, Ha M, Manno M, Frisbie CD, Leighton C. 2012. Hopping transport and the Hall effect near the insulator-metal transition in electrochemically gated poly(3-hexylthiophene) transistors. *Nat. Commun.* 3(1):1210
16. Hallinan DT, Balsara NP. 2013. Polymer electrolytes. *Annu. Rev. Mater. Res.* 43:503–25
17. Albinsson I, Mellander B-E, Stevens JR. 1992. Ionic conductivity in poly(propylene glycol) complexed with lithium and sodium triflate. *J. Chem. Phys.* 96(1):681–90
18. Newman J, Thomas-Alyea KE. 2004. *Electrochemical Systems*. Hoboken, NJ: Wiley-Interscience. 3rd ed.
19. Volkov AV, Wijeratne K, Mitraka E, Ail U, Zhao D, et al. 2017. Understanding the capacitance of PEDOT:PSS. *Adv. Funct. Mater.* 27(28):1700329
20. Buck RP. 1989. General voltage-step responses and impedances of mixed-conductor films and diodes: metal-contact cells with mobile anions or cations. *J. Phys. Chem.* 93(16):6212–19
21. Buck RP. 1988. Electron hopping in one dimension: mixed conductor membranes. *J. Phys. Chem.* 92(14):4196–200
22. Nahir TM, Buck RP. 1993. Transport processes in membranes containing neutral ion carriers, positive ion complexes, negative mobile sites, and ion pairs. *J. Phys. Chem.* 97(47):12363–72
23. Rawlings D, Thomas EM, Segalman RA, Chabynyc ML. 2019. Controlling the doping mechanism in poly(3-hexylthiophene) thin-film transistors with polymeric ionic liquid dielectrics. *Chem. Mater.* 31(21):8820–29
24. Mills T, Kaake LG, Zhu X-Y. 2009. Polaron and ion diffusion in a poly(3-hexylthiophene) thin-film transistor gated with polymer electrolyte dielectric. *Appl. Phys. A* 95(1):291–96

25. Kaneto K, Agawa H, Yoshino K. 1987. Cycle life, stability, and characteristics of color switching cells utilizing polythiophene films. *J. Appl. Phys.* 61(3):1197–205
26. Bischak CG, Flagg LQ, Yan K, Rehman T, Davies DW, et al. 2020. A reversible structural phase transition by electrochemically-driven ion injection into a conjugated polymer. *J. Am. Chem. Soc.* 142(16):7434–42
27. Bocharova V, Sokolov AP. 2020. Perspectives for polymer electrolytes: a view from fundamentals of ionic conductivity. *Macromolecules* 53(11):4141–57
28. Wang Y, Fan F, Agapov AL, Yu X, Hong K, et al. 2014. Design of superionic polymers—new insights from Walden plot analysis. *Solid State Ionics* 262:782–84
29. Cohen MH, Turnbull D. 1959. Molecular transport in liquids and glasses. *J. Chem. Phys.* 31(5):1164–69
30. Turnbull D, Cohen MH. 1970. On the free-volume model of the liquid-glass transition. *J. Chem. Phys.* 52(6):3038–41
31. Ratner MA, Nitzan A. 1989. Conductivity in polymer ionics. Dynamic disorder and correlation. *Faraday Discuss. Chem. Soc.* 88:19–42
32. Boden N, Leng SA, Ward IM. 1991. Ionic conductivity and diffusivity in polyethylene oxide/electrolyte solutions as models for polymer electrolytes. *Solid State Ionics* 45(3):261–70
33. Aziz SB, Woo TJ, Kadir MFZ, Ahmed HM. 2018. A conceptual review on polymer electrolytes and ion transport models. *J. Sci. Adv. Mater. Devices* 3(1):1–17
34. Chung SH, Such K, Wiecek W, Stevens JR. 1994. An analysis of ionic conductivity in polymer electrolytes. *J. Polym. Sci. B Polym. Phys.* 32(16):2733–41
35. Choo Y, Halat DM, Villaluenga I, Timachova K, Balsara NP. 2020. Diffusion and migration in polymer electrolytes. *Prog. Polym. Sci.* 103:101220
36. Meyer WH. 1998. Polymer electrolytes for lithium-ion batteries. *Adv. Mater.* 10(6):439–48
37. Mao G, Saboungi M-L, Price DL, Armand M, Mezei F, Pouget S. 2002.  $\alpha$ -Relaxation in PEO–LiTFSI polymer electrolytes. *Macromolecules* 35(2):415–19
38. Loo WS, Mongcopa KI, Gribble DA, Faraone AA, Balsara NP. 2019. Investigating the effect of added salt on the chain dimensions of poly(ethylene oxide) through small-angle neutron scattering. *Macromolecules* 52(22):8724–32
39. Mongcopa KIS, Tyagi M, Mailoa JP, Samsonidze G, Kozinsky B, et al. 2018. Relationship between segmental dynamics measured by quasi-elastic neutron scattering and conductivity in polymer electrolytes. *ACS Macro Lett.* 7(4):504–8
40. Hall LM, Seitz ME, Winey KI, Opper KL, Wagener KB, et al. 2012. Ionic aggregate structure in ionomer melts: effect of molecular architecture on aggregates and the ionomer peak. *J. Am. Chem. Soc.* 134(1):574–87
41. Yan L, Rank C, Mecking S, Winey KI. 2020. Gyroid and other ordered morphologies in single-ion conducting polymers and their impact on ion conductivity. *J. Am. Chem. Soc.* 142(2):857–66
42. Yan L, Bustillo KC, Panova O, Minor AM, Winey KI. 2018. Solution-grown crystals of precise acid- and ion-containing polyethylenes. *Polymer* 135:111–19
43. Young W-S, Epps TH. 2009. Salt doping in PEO-containing block copolymers: counterion and concentration effects. *Macromolecules* 42(7):2672–78
44. Singh M, Odusanya O, Wilmes GM, Eitouni HB, Gomez ED, et al. 2007. Effect of molecular weight on the mechanical and electrical properties of block copolymer electrolytes. *Macromolecules* 40(13):4578–85
45. Xie S, Meyer DJ, Wang E, Bates FS, Lodge TP. 2019. Structure and properties of bicontinuous microemulsions from salt-doped ternary polymer blends. *Macromolecules* 52(24):9693–702
46. Knychala P, Banaszak M. 2014. Simulations on a swollen gyroid nanostructure in thin films relevant to systems of ionic block copolymers. *Eur. Phys. J. E* 37(7):67
47. Park MJ, Balsara NP. 2008. Phase behavior of symmetric sulfonated block copolymers. *Macromolecules* 41(10):3678–87
48. Coropceanu V, Cornil J, da Silva Filho DA, Olivier Y, Silbey R, Brédas J-L. 2007. Charge transport in organic semiconductors. *Chem. Rev.* 107(4):926–52
49. Jacobs IE, Moulé AJ. 2017. Controlling molecular doping in organic semiconductors. *Adv. Mater.* 29(42):1703063
50. Baranovskii SD. 2014. Theoretical description of charge transport in disordered organic semiconductors. *Phys. Status Solidi B* 251(3):487–525

51. Thomas EM, Popere BC, Fang H, Chabiny ML, Segalman RA. 2018. Role of disorder induced by doping on the thermoelectric properties of semiconducting polymers. *Chem. Mater.* 30(9):2965–72
52. Zuo G, Abdalla H, Kemerink M. 2016. Impact of doping on the density of states and the mobility in organic semiconductors. *Phys. Rev. B* 93(23):235203
53. Yee PY, Scholes DT, Schwartz BJ, Tolbert SH. 2019. Dopant-induced ordering of amorphous regions in regiorandom P3HT. *J. Phys. Chem. Lett.* 10(17):4929–34
54. Duong DT, Toney MF, Salleo A. 2012. Role of confinement and aggregation in charge transport in semicrystalline polythiophene thin films. *Phys. Rev. B* 86(20):205205
55. Patel SN, Glauddell AM, Peterson KA, Thomas EM, O'Hara KA, et al. 2017. Morphology controls the thermoelectric power factor of a doped semiconducting polymer. *Sci. Adv.* 3(6):e1700434
56. Thomas EM, Brady MA, Nakayama H, Popere BC, Segalman RA, Chabiny ML. 2018. X-ray scattering reveals ion-induced microstructural changes during electrochemical gating of poly(3-hexylthiophene). *Adv. Funct. Mater.* 28(44):1803687
57. Liu W, Müller L, Ma S, Barlow S, Marder SR, et al. 2018. Origin of the  $\pi$ - $\pi$  spacing change upon doping of semiconducting polymers. *J. Phys. Chem. C* 122(49):27983–90
58. Thelen JL, Wu S-L, Javier AE, Srinivasan V, Balsara NP, Patel SN. 2015. Relationship between mobility and lattice strain in electrochemically doped poly(3-hexylthiophene). *ACS Macro Lett.* 4(12):1386–91
59. Kroon R, Kiefer D, Stegerer D, Yu L, Sommer M, Müller C. 2017. Polar side chains enhance processability, electrical conductivity, and thermal stability of a molecularly p-doped polythiophene. *Adv. Mater.* 29(24):1700930
60. Liu J, Qiu L, Alessandri R, Qiu X, Portale G, et al. 2018. Enhancing molecular n-type doping of donor-acceptor copolymers by tailoring side chains. *Adv. Mater.* 30(7):1704630
61. Aubry TJ, Axtell JC, Basile VM, Winchell KJ, Lindemuth JR, et al. 2019. Dodecaborane-based dopants designed to shield anion electrostatics lead to increased carrier mobility in a doped conjugated polymer. *Adv. Mater.* 31(11):1805647
62. Giovannitti A, Maria IP, Hanifi D, Donahue MJ, Bryant D, et al. 2018. The role of the side chain on the performance of n-type conjugated polymers in aqueous electrolytes. *Chem. Mater.* 30(9):2945–53
63. Hynynen J, Kiefer D, Yu L, Kroon R, Munir R, et al. 2017. Enhanced electrical conductivity of molecularly p-doped poly(3-hexylthiophene) through understanding the correlation with solid-state order. *Macromolecules* 50(20):8140–48
64. Lim E, Glauddell AM, Miller R, Chabiny ML. 2019. The role of ordering on the thermoelectric properties of blends of regioregular and regiorandom poly(3-hexylthiophene). *Adv. Electron. Mater.* 5(11):1800915
65. Collins BA, Cochran JE, Yan H, Gann E, Hub C, et al. 2012. Polarized X-ray scattering reveals non-crystalline orientational ordering in organic films. *Nat. Mater.* 11(6):536–43
66. Patel SN, Glauddell AM, Kiefer D, Chabiny ML. 2016. Increasing the thermoelectric power factor of a semiconducting polymer by doping from the vapor phase. *ACS Macro Lett.* 5(3):268–72
67. Gu K, Snyder CR, Onorato J, Luscombe CK, Bosse AW, Loo Y-L. 2018. Assessing the Huang-Brown description of tie chains for charge transport in conjugated polymers. *ACS Macro Lett.* 7(11):1333–38
68. Himmelberger S, Vandewal K, Fei Z, Heeney M, Salleo A. 2014. Role of molecular weight distribution on charge transport in semiconducting polymers. *Macromolecules* 47(20):7151–57
69. Mindemark J, Lacey MJ, Bowden T, Brandell D. 2018. Beyond PEO—alternative host materials for Li<sup>+</sup>-conducting solid polymer electrolytes. *Prog. Polym. Sci.* 81:114–43
70. MacFarlane DR, Forsyth M, Izgorodina EI, Abbott AP, Annat G, Fraser K. 2009. On the concept of ionicity in ionic liquids. *Phys. Chem. Chem. Phys.* 11(25):4962–67
71. Hayashi A, Noi K, Sakuda A, Tatsumisago M. 2012. Superionic glass-ceramic electrolytes for room-temperature rechargeable sodium batteries. *Nat. Commun.* 3(1):856
72. Chiang CK, Fincher CR, Park YW, Heeger AJ, Shirakawa H, et al. 1977. Electrical conductivity in doped polyacetylene. *Phys. Rev. Lett.* 39(17):1098–101
73. Vijayakumar V, Zhong Y, Untilova V, Bahri M, Herrmann L, et al. 2019. Bringing conducting polymers to high order: toward conductivities beyond 105 S cm<sup>-1</sup> and thermoelectric power factors of 2 mW m<sup>-1</sup> K<sup>-2</sup>. *Adv. Energy Mater.* 9(24):1900266
74. Pingel P, Neher D. 2013. Comprehensive picture of  $\rho$ -type doping of P3HT with the molecular acceptor F<sub>4</sub>TCNQ. *Phys. Rev. B* 87(11):115209

75. Jamnik J, Maier J. 2001. Generalised equivalent circuits for mass and charge transport: chemical capacitance and its implications. *Phys. Chem. Chem. Phys.* 3(9):1668–78
76. Kim Y, Han M, Kim J, Kim E. 2018. Electrochromic capacitive windows based on all conjugated polymers for a dual function smart window. *Energy Environ. Sci.* 11(8):2124–33
77. Simon DT, Gabrielsson EO, Tybrandt K, Berggren M. 2016. Organic bioelectronics: bridging the signaling gap between biology and technology. *Chem. Rev.* 116(21):13009–41
78. Zhao D, Fabiano S, Berggren M, Crispin X. 2017. Ionic thermoelectric gating organic transistors. *Nat. Commun.* 8(1):14214
79. Moser M, Hidalgo TC, Surgailis J, Gladisch J, Ghosh S, et al. 2020. Side chain redistribution as a strategy to boost organic electrochemical transistor performance and stability. *Adv. Mater.* 32(37):2002748
80. Gladisch J, Stavrinidou E, Ghosh S, Giovannitti A, Moser M, et al. 2019. Reversible electronic solid–gel switching of a conjugated polymer. *Adv. Sci.* 7(2):1901144
81. Friedlein JT, Donahue MJ, Shaheen SE, Malliaras GG, McLeod RR. 2016. Microsecond response in organic electrochemical transistors: exceeding the ionic speed limit. *Adv. Mater.* 28(38):8398–404
82. Berggren M, Malliaras GG. 2019. How conducting polymer electrodes operate. *Science* 364(6437):233–34
83. Ma Y, Doyle M, Fuller TF, Doeff MM, Jonghe LCD, Newman J. 1995. The measurement of a complete set of transport properties for a concentrated solid polymer electrolyte solution. *J. Electrochem. Soc.* 142(6):1859–68
84. Schausner NS, Seshadri R, Segalman RA. 2019. Multivalent ion conduction in solid polymer systems. *Mol. Syst. Des. Eng.* 4(2):263–79
85. Klett M, Giesecke M, Nyman A, Hallberg F, Lindström RW, et al. 2012. Quantifying mass transport during polarization in a Li ion battery electrolyte by in situ <sup>7</sup>Li NMR imaging. *J. Am. Chem. Soc.* 134(36):14654–57
86. Choi J-H, Xie W, Gu Y, Frisbie CD, Lodge TP. 2015. Single ion conducting, polymerized ionic liquid triblock copolymer films: high capacitance electrolyte gates for n-type transistors. *ACS Appl. Mater. Interfaces* 7(13):7294–302
87. Patel SN, Javier AE, Stone GM, Mullin SA, Balsara NP. 2012. Simultaneous conduction of electronic charge and lithium ions in block copolymers. *ACS Nano* 6(2):1589–600
88. Christie AM, Lilley SJ, Staunton E, Andreev YG, Bruce PG. 2005. Increasing the conductivity of crystalline polymer electrolytes. *Nature* 433(7021):50–53
89. Inal S, Rivnay J, Leleux P, Ferro M, Ramuz M, et al. 2014. A high transconductance accumulation mode electrochemical transistor. *Adv. Mater.* 26(44):7450–55
90. Beekingham BS, Ho V, Segalman RA. 2014. Formation of a rigid amorphous fraction in poly(3-(2'-ethyl)hexylthiophene). *ACS Macro Lett.* 3(7):684–88
91. Thomas EM, Peterson KA, Balzer AH, Rawlings D, Stingelin N, et al. 2020. Effects of counter-ion size on delocalization of carriers and stability of doped semiconducting polymers. *Adv. Electron. Mater.* 6(12):2000595
92. Kiefer D, Kroon R, Hofmann AI, Sun H, Liu X, et al. 2019. Double doping of conjugated polymers with monomer molecular dopants. *Nat. Mater.* 18(2):149–55
93. Mazaheripour A, Thomas EM, Segalman RA, Chabynyc ML. 2019. Nonaggregating doped polymers based on poly(3,4-propylenedioxythiophene). *Macromolecules* 52(5):2203–13
94. O'Connor B, Kline RJ, Conrad BR, Richter LJ, Gundlach D, et al. 2011. Anisotropic structure and charge transport in highly strain-aligned regioregular poly(3-hexylthiophene). *Adv. Funct. Mater.* 21(19):3697–705
95. Ashizawa M, Zheng Y, Tran H, Bao Z. 2019. Intrinsically stretchable conjugated polymer semiconductors in field effect transistors. *Prog. Polym. Sci.* 100:101181
96. Kelly T, Ghadi BM, Berg S, Ardebili H. 2016. *In situ* study of strain-dependent ion conductivity of stretchable polyethylene oxide electrolyte. *Sci. Rep.* 6:20128
97. Reynolds VG, Oh S, Xie R, Chabynyc ML. 2020. Model for the electro-mechanical behavior of elastic organic transistors. *J. Mater. Chem. C* 8(27):9276–85
98. Wirix MJM, Bomans PHH, Friedrich H, Sommerdijk NAJM, de With G. 2014. Three-dimensional structure of P3HT assemblies in organic solvents revealed by cryo-TEM. *Nano Lett.* 14(4):2033–38
99. Khodagholy D, Rivnay J, Sessolo M, Gurfinkel M, Leleux P, et al. 2013. High transconductance organic electrochemical transistors. *Nat. Commun.* 4(1):2133